the FEBS Journal

The multicopper oxidase from the archaeon *Pyrobaculum aerophilum* shows nitrous oxide reductase activity

André T. Fernandes[1], João M. Damas[1], Smilja Todorovic[1], Robert Huber[2], M. Camilla Baratto[3], Rebecca Pogni[3], Cláudio M. Soares[1] and Lígia O. Martins[1]

1 Instituto de Tecnologia Química e Biológica, Universidade Nova de Lisboa, Oeiras, Portugal
2 Kommunale Berufsfachschule für biologisch-technische Assistenten, Straubing, Germany
3 Department of Chemistry, University of Siena, Italy

Keywords
Archaea; hyperthermophiles; multicopper oxidases; nitrous oxide reductase; *Pyrobaculum aerophilum*

Correspondence
L. O. Martins, Instituto de Tecnologia Química e Biológica, Universidade Nova de Lisboa, Av. da República, 2781-901 Oeiras, Portugal
Fax: +351 214411277
Tel: +351 214469534
E-mail: lmartins@itqb.unl.pt

(Received 13 April 2010, revised 25 May 2010, accepted 28 May 2010)

doi:10.1111/j.1742-4658.2010.07725.x

The multicopper oxidase from the hyperthermophilic archaeon *Pyrobaculum aerophilum* (McoP) was overproduced in *Escherichia coli* and purified to homogeneity. The enzyme consists of a single 49.6 kDa subunit, and the combined results of UV–visible, CD, EPR and resonance Raman spectroscopies showed the characteristic features of the multicopper oxidases. Analysis of the McoP sequence allowed its structure to be derived by comparative modeling methods. This model provided a criterion for designing meaningful site-directed mutants of the enzyme. McoP is a hyperthermoactive and thermostable enzyme with an optimum reaction temperature of 85 °C, a half-life of inactivation of ~ 6 h at 80 °C, and temperature values at the midpoint from 97 to 112 °C. McoP is an efficient metallo-oxidase that catalyzes the oxidation of cuprous and ferrous ions with turnover rate constants of 356 and 128 min^{-1}, respectively, at 40 °C. It is noteworthy that McoP follows a ping-pong mechanism, with three-fold higher catalytic efficiency when using nitrous oxide as electron acceptor than when using dioxygen, the typical oxidizing substrate of multicopper oxidases. This finding led us to propose that McoP represents a novel archaeal nitrous oxide reductase that is most probably involved in the final step of the denitrification pathway of *P. aerophilum*.

Introduction

Multicopper oxidases (MCOs) are a large family of enzymes that couple the one-electron oxidation of substrates with the four-electron reduction of molecular oxygen to water [1,2]. This family is unique among copper proteins since its members contain one of each of the three types of biological copper sites, type 1 (T1), type 2 (T2) and the binuclear type 3 (T3). The T1 site is characterized by an intense $S(\pi) \rightarrow Cu(d_{x^2-y^2})$ charge transfer (CT) absorption band at ~ 600 nm, which is responsible for the intense blue color of these enzymes, and a narrow parallel hyperfine splitting [$A_{||}$ = (43–90) × 10^{-4} cm^{-1}] in the EPR spectra. This is the site of substrate oxidation, and in this respect the MCO family can be separated into two

Abbreviations
ABTS, 2,2′-azinobis-(3-ethylbenzo-6-thiazolinesulfonic acid); CT, charge transfer; DSC, differential scanning calorimetry; MCO, multicopper oxidase; McoP, multicopper oxidase from *Pyrobaculum aerophilum*; N_2OR, nitrous oxide reductase; RR, resonance Raman; SGZ, syringaldazine; T1, type 1; T2, type 2; T3, type 3.

classes: enzymes that oxidize aromatic substrates with high efficiency, i.e. laccases, and those that oxidize metal ion substrates, or metallo-oxidases. The trinuclear center, where dioxygen is reduced to water, is comprised of two T3 copper ions and one T2 copper ion. The two T3 copper ions, which are usually antiferromagnetically coupled through a bridging ligand and therefore EPR silent, show a characteristic absorption band at 330 nm. The T2 site lacks strong absorption bands, and exhibits a large parallel hyperfine splitting in the EPR spectra [$A_{||} = (150–201) \times 10^{-4}$ cm^{-1}]. MCOs are widely distributed throughout nature, and play essential roles in the physiology of almost all aerobes.

In recent years, we have focused our attention on the study of prokaryotic MCOs, the CotA laccase from *Bacillus subtilis* and the metallo-oxidase McoA from *Aquifex aeolicus*, because of their potential for biotechnological application [3–8]. Several structure–function relationship studies have been performed, revealing redox properties of the T1 site and providing structural insights into the principal stages of the mechanism of dioxygen reduction at the trinuclear center [9–12]. Enzymes from extremophiles and thermophiles, in particular, are promising for industrial applications, as they have high intrinsic thermal and chemical stability. The search for MCOs, among the genomes of hyperthermophilic archaeons sequenced so far, revealed that *Pyrobaculum aerophilum* is the only microorganism that possesses an MCO-like enzyme, encoded by the *PAE1888* gene [13]. Therefore, in this work we set out to fully characterize this archaeal enzyme. Additional interest in this enzyme arose from a recent report on the transcriptional patterns of *P. aerophilum* upon cultivation in the presence of oxygen, nitrate, arsenate and ferric ions that suggested its putative involvement in the last step of the denitrification pathway of this microorganism [14]. This would represent a completely new function among the MCOs. *P. aerophilum* is a microaerophilic, chemoautotrophic microorganism that is recognized for its respiratory versatility being capable of using several organic, as well as inorganic, compounds as substrates during aerobic or anaerobic respiration [14–16]. It is the only hyperthermophilic denitrifier that has been characterized so far [17–19]. The reduction of nitrate to dinitrogen gas is accomplished by different types of metalloenzymes in four steps: nitrate to nitrite, nitrite to nitric oxide, nitric oxide to nitrous oxide, and finally nitrous oxide to dinitrogen [20,21]. The nitrate and nitric oxide reductases of *P. aerophilum* have been isolated and biochemically characterized, and the gene coding for a heme O-containing nitric oxide reductase was identified in its genome [13,18,22]. However, no recognizable homolog of *nosZ*, which codes for nitrous oxide reductase (N_2OR) in bacteria, has been found in the genome of this archaeon, indicating the existence of an alternative and unknown N_2OR. This hypothesis was also raised for other bacterial and archaeal strains that reduce nitrous oxide and lack identified N_2OR genes [23].

This study describes the purification and biochemical and structural characterization (based on the comparative model) of the first hyperthermophilic archaeal-type metallo-oxidase, designated McoP (multicopper oxidase from *P. aerophilum*). Indeed, whereas MCOs, both laccases and metallo-oxidases, are well characterized in eukaryotes and bacteria, only one archaeal laccase has been described so far [24]. Although the recombinant purified McoP is similar in several respects to other well-characterized MCOs, it is unique in terms of being the first MCO that uses nitrous oxide more efficiently than dioxygen as an oxidizing substrate. Overall, our results reinforce the prediction of Cozen *et al.* [14] that McoP is involved in the denitrification pathway of *P. aerophilum*, and thus represents a novel N_2OR.

Results

Biochemical, spectroscopic and structural characterization of recombinant McoP

Sequence alignment of *P. aerophilum* McoP with CueO from *Escherichia coli* and CotA laccase from *B. subtilis* clearly indicates that this enzyme is a member of the MCO family of enzymes (Fig. 1). The MCO sequence motif pattern, which contains the four elements that together form the copper-binding sites in the protein, is conserved in McoP, including a Met corresponding to the axial position of the T1 copper in other MCOs. Furthermore, McoP has in its sequence a predicted TAT-dependent putative signal peptide, indicating that this protein should be exported to the space between the cytoplasmic membrane and the external protein surface layer [19]. The *mcop* gene encodes a protein with 477 amino acids and a predicted molecular mass of 52.9 kDa. The gene was cloned into the expression vector pET-15b to make pATF-20, and the final construct was transformed into *E. coli* Tuner (DE3). The recombinant McoP was purified to homogeneity by using metal affinity and exclusion chromatography, and gave a single band of $\sim$ 52 kDa in SDS/PAGE (Table S1 and Fig. S1). Size exclusion chromatography yielded a native molecular mass of 49.6 kDa. The as-isolated enzyme was found to be partially copper depleted, containing 3.2 mol of copper per mol of protein instead of the expected 4 : 1 ratio. The UV–visible spectrum of

Fig. 1. Sequence alignment of McoP with CotA laccase from *Bacillus subtilis* (1GSK) and CueO from *Escherichia coli* (1KV7). The alignment was generated by using the primary sequences of the respective proteins. The copper ligands of MCOs (gray boxes) are all conserved in McoP. Two dots indicate similarity, and an asterisk indicates identity.

McoP showed the spectroscopic characteristics of the MCOs, with a CT absorption band at approximately 600 nm, originating from the T1 Cu–S(Cys) bond, and a small shoulder at 330 nm, characteristic of a bridging ligand between the T3 copper ions (Fig. 2A). The CD spectrum of McoP reflected the typical secondary structure of MCOs, rich in β-sheets, with a negative peak at $\sim$ 213 nm (Fig. S2). A secondary structure estimate based on the CDSSTR method yielded values of 6% in α-helices, 30% in β-sheets, and more than 60% in turns and random coils [25]. The resonance Raman (RR) spectrum (Fig. 2B) revealed a number of vibrational modes in the low-frequency region, originating from the coupling of the Cu–S(Cys) stretch with the S–C_β–C_α(Cys) bond, as typically observed in copper proteins containing a T1 site [12,26,27]. The intensity-weighted frequency $< \nu_{Cu-S} >$ of all Cu–S stretching modes, which is inversely proportional to the Cu–S(Cys) bond length in the T1 site, was 406 cm^{-1} [12,26,27]. A relatively small value of $< \nu_{Cu-S} >$ correlates well with the low redox potential of the T1 site [E^0 (T1) = 398 mV] [12,26,27], determined by the disappearance of the CT absorption band in the 500–800 nm region (Fig. 3). The X-band EPR spectrum of the as-isolated McoP paired to its simulation (Fig. 4A) revealed values of the magnetic parameters, $g_{||} = 2.224 \pm 0.001$ and $A_{||} = (71.6 \pm 1) \times 10^{-4}$ cm^{-1}, that fall within the range of the T1 copper contribution. No evidence for the characteristic resonances of the T2 site were present in the spectrum [28,29]. A new set of resonances with spin Hamiltonian magnetic parameters typical for a T2 copper center [$g_{||} = 2.258 \pm 0.001$ and $A_{||} = (183.4 \pm 1) \times 10^{-4}$ cm^{-1}] appeared in the spectrum after addition of exogenous copper (Fig. 4B,C). Overall, the analysis of EPR spectra suggests that the as-isolated McoP is in a T2-depleted form, which is in accordance with the lower copper/protein ratio measured in the protein and the requirement for exogenous copper to achieve full activity (see below).

The crystal structures of CueO from *E. coli* and CotA from *B. subtilis* were used to derive a structural model for McoP by comparative modeling techniques (Fig. 5A). As expected, the model revealed the same overall fold of MCOs, assembled from three cupredoxin domains, as the structures used as templates. The active sites of MCOs are highly conserved, and include a His-Cys-His triad, which forms a Cys–His bond bridging the T1 and T3 copper ions; this triad is likely to provide the route of the intramolecular electron transfer from the T1 copper to the T3 binuclear cluster during substrate turnover (illustrated in Fig. 5B). The analysis of the model suggests that the T1 site in McoP is less exposed than in CotA [3], but not so buried as in CueO, in which it is occluded by a Met-rich helix and loop (Fig. 5C) [31]. The residues contributing to the semiocclusion of this site in McoP are Trp355 (which replaces Asn408 in CueO and Leu386 in CotA), Met389 (structurally equivalent to Met441 of CueO), and Met297 (in a similar position to Met303 of CueO) (Fig. 5D). Furthermore, there is a negatively charged residue in the neighborhood of the T1 site, Glu296 (in a similar position to Gln302 of CueO), which is semiburied in the binding pocket and 7.75 Å from the T1 copper atom (Fig. 5D).

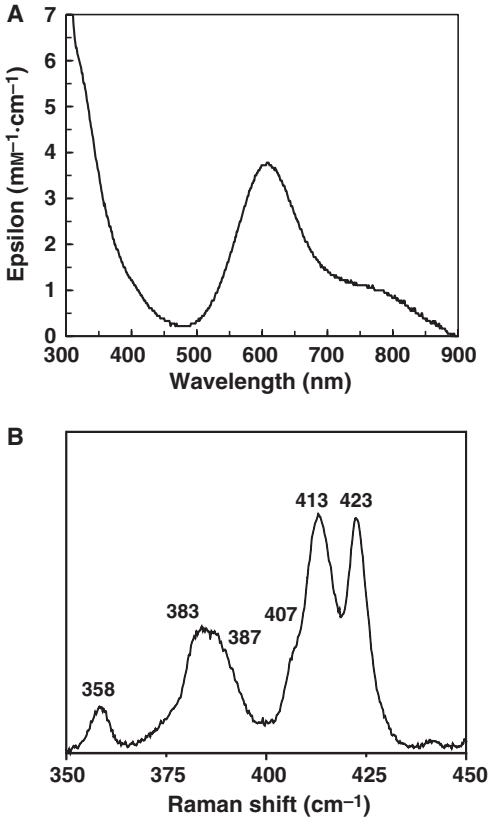

Fig. 2. (A) UV–visible spectrum of the as-isolated recombinant McoP. (B) RR spectrum of 2 mM McoP, measured with 568 nm excitation, 5 mW laser power, and 40 s accumulation time, at 77 K.

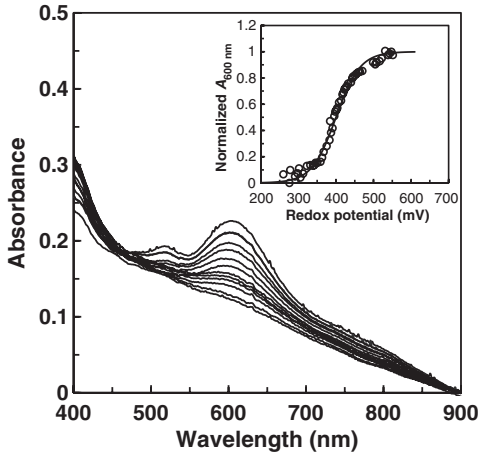

Fig. 3. Redox potential determination. UV–visible spectra of McoP (50 μM) in 20 mM Tris/HCl buffer (pH 7.6) obtained along the redox titration. Inset: titration curve followed at 600 nm. The line corresponds to a fitting to the sequential equilibrium of a one-electron step.

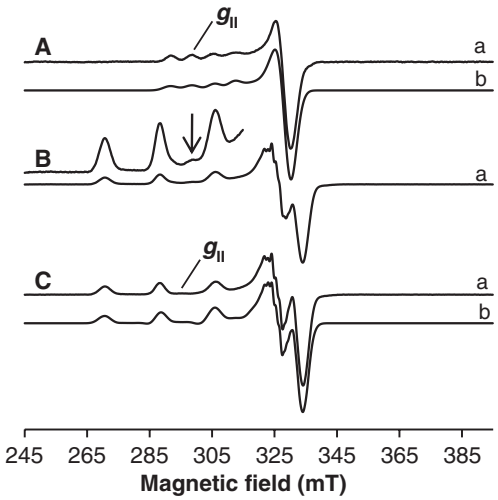

Fig. 4. X-band EPR spectrum of (A) the as-isolated McoP (a) paired to its simulation (b) and (B) after incubation with five equivalents of Cu^{2+}. The contribution of T1 copper is present in both spectra, as indicated by the arrow. (C) Experimental spectrum of the McoP incubated with Cu^{2+} subtracted from the as-isolated McoP (a) paired to its simulation (b), where the contribution of T2 copper is evident.

McoP is a thermoactive and hyperthermostable enzyme

As expected for a hyperthermophilic enzyme, McoP showed a reaction optimum temperature of ~ 85 °C (Fig. 6), which is comparable to that of the *Thermus thermophilus* laccase [32] and *A. aeolicus* metallooxidase [5,32], and close to the optimal temperature for *P. aerophilum* growth [19]. McoP reveals intrinsic hyperthermostability, as shown by kinetic stability measurements at 80 °C, which allow determination of the amount of enzyme that loses activity irreversibly. The enzyme deactivates according to first-order kinetics, and a half-life of inactivation of 330 min (5.5 h) was calculated (Fig. 7A and insert). This shows that McoP is a robust catalyst, although to a lower extent than McoA from *A. aeolicus* [5] and the laccase from *T. thermophilus* [32]. The first-order deactivation kinetics can be described by the classical Lumry–Eyring model (N↔U → D, where N, U and D are the native, the reversibly unfolded and the irreversibly denatured enzyme), pointing to a simple pathway of unfolding and deactivation. The thermal stability was further probed by differential scanning calorimetry (DSC). The DSC thermogram (Fig. 7B) reveals a complex process, as the excess heat capacity profile can only be fitted using a non-two-state model with three independent transitions [4]. The midpoint temperatures at each transition clearly reflect the high

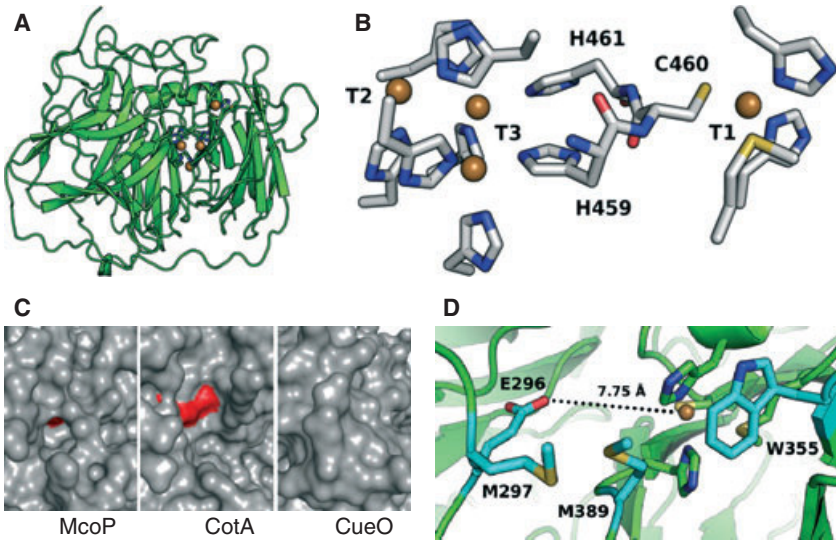

Fig. 5. (A) Overall fold and copper centers of McoP. The protein is shown in cartoon representation, with the copper-coordinating residues as sticks and the copper ions as spheres. (B) T1 and T2/T3 site coordinating residues. The side chain residues of copper centers are shown in stick representation. The His459-Cys460-His461 triad bridges the T1 and T3 sites. (C) Comparison of binding pocket of the McoP model with CotA and CueO structures. The proteins are shown in surface representation. The T1 site contribution to this surface is highlighted in red. (D) Close-up of the binding pocket near the T1 site of McoP. The T1 copper-binding residue side chains are shown in stick representation. The occluding Met297, Met389 and Trp355, as well as the semiburied Glu296, are also shown in stick representation and highlighted in cyan. This figure was prepared with PYMOL [30].

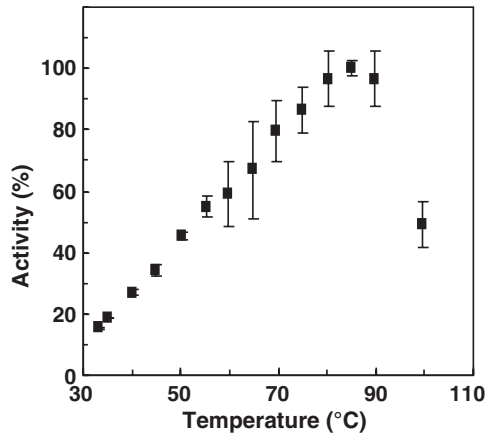

Fig. 6. Temperature dependence of recombinant McoP activity.

stability of McoP: 96.6 °C (± 0.7 °C), 101.5 °C (± 0.4 °C), and 112.2 °C (± 0.4 °C). Similarly, three transitions were previously used to describe unfolding profiles of plant ascorbate oxidase [33], human ceruloplasmin [34], CotA laccase from *B. subtilis* [35], and McoA from *A. aeolicus* [4], and they apparently correlate with a structural organization of three cupredoxin-like domains for the ascorbate oxidase, CotA laccase, and McoA, and six cupredoxin domains organized into three pairs in human ceruloplasmin [1].

McoP is a metallo-oxidase

The catalytic properties of McoP were measured with standard substrates in the presence of oxygen: (a) two aromatic reducing substrates [2,2′-azinobis-(3-ethylbenzo-6-thiazolinesulfonic acid)] (ABTS) and the phenolic syringaldazine (SGZ); and (b) two metal reducing substrates, Cu^{+} and Fe^{2+}. The activity tested in the presence of various concentrations of exogenous copper (10–1000 μM $CuCl_2$) revealed that 100 μM $CuCl_2$ enhanced enzymatic rates two-fold, and all activities were therefore measured in the presence of this copper concentration. Overall, the pH profiles for aromatics are similar to those of other characterized MCOs [36], displaying the typical monotonic decrease for ABTS with maximal activity at pH 3, and a bell-shaped profile with an optimum at pH 7 for SGZ oxidation (data not shown). The enzyme showed Cu^{+}/Fe^{2+} oxidation kinetics that followed the Michaelis–Menten model, with two-fold to 10-fold higher efficiencies for Cu^{+} and Fe^{2+} as compared with the tested aromatic compounds, Fe^{2+} being the favored substrate (Table 1). The metal oxidation efficiencies (k_{cat}/K_m), measured at 40 °C, were equivalent to those reported for other members of the MCO family [5,37–39]. Nevertheless, considering that at 40 °C only 30% of the maximal activity is achieved (Fig. 6), McoP can be considered to be quite a remarkable catalyst at the optimum

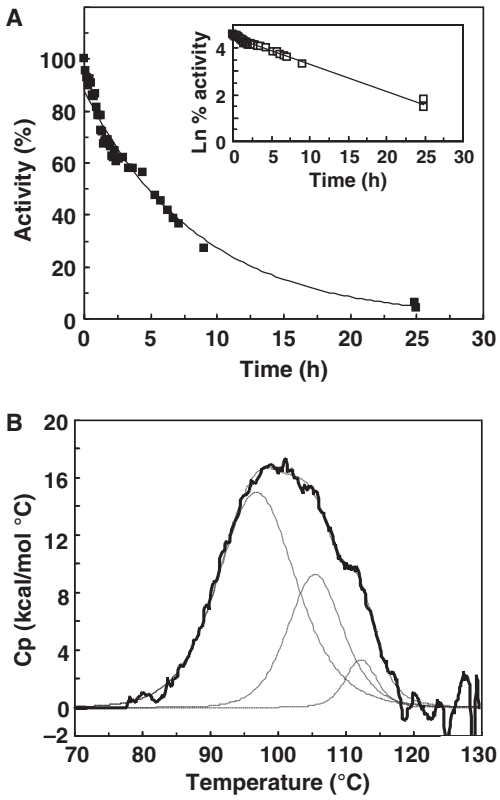

Fig. 7. (A) Kinetic stability of McoP. The activity decay at 80 °C was fitted accurately, considering an exponential decay (the solid line shows the fit) with a half-life of 330 min. The inset clearly shows that the activity decay of McoP can be fitted to a single first-order process, as the logarithm of activity displays an inverse linear relationship with time. (B) DSC of McoP. Excess heat capacity obtained from the DSC scan (at pH 3) of McoP. The thick line (experimental data) was fitted with three independent transitions, shown separately as thin lines, with melting temperatures of 96.6, 101.5, and 112.2 °C.

Table 1. Steady-state apparent kinetic parameters of McoP. Reactions were performed in the presence of 0.1 mM $CuCl_2$ and at 40 °C [30% of the maximal activity (see Fig. 6)].

Substrate	$K_{m\ app}$ (μM)	$k_{cat\ app}$ (min^{-1})	k_{cat}/K_m ($M^{-1}·s^{-1}$)
Cu^+	124 ± 22	354 ± 30	4.8×10^4
Fe^{2+}	22 ± 2	126 ± 6	9.6×10^4
ABTS	133 ± 8	72 ± 6	0.9×10^4
SGZ	14 ± 5	24 ± 0	2.9×10^4

temperature, with efficiencies of 1.6×10^5 and 3.2×10^5 $M^{-1}·s^{-1}$ for Cu^+ and Fe^{2+}, respectively.

As substrate oxidation occurs via the T1 site, substrate specificity is conferred by structure–activity relationships near this site [40]. Guided by the structure obtained by comparative modeling, site-directed mutagenesis was used to replace Trp355, Met297 and Met389 (Fig. 5D) with Ala, to test the hypothesis that these residues could: (a) hinder the access of bulky substrates; or (b) in the case of Met residues, provide a pathway for electron transfer from the metal substrates to the T1 site, as shown for CueO [31]. We showed that these mutations resulted in proteins exhibiting similar biochemical and spectroscopic properties to those of the wild type (Table 2). For the Met and Glu296 mutants, slight differences in the enzymatic efficiencies (two- to three-fold lower) were found for the larger aromatic compounds, whereas these values remained basically unchanged for the smaller metal substrates (Table 3). These changes are most probably associated with minor alterations in the neighborhood of the T1 site. Overall, we concluded that the individual mutated residues do not contribute appreciably to the substrate specificity of McoP.

McoP displays one of the lowest redox potential values (Fig. 3) among MCOs, ranging from 340 mV for ascorbate oxidase to 790 mV for some fungal laccases [2]. We showed by site-directed mutagenesis that this value is at least partially correlated with the proximity of Glu296 (Fig. 5D), as its replacement by a Gln resulted in an increase of the redox potential by 30 mV (Table 2). Therefore, the presence of this negative charge in the T1 neighborhood most likely contributes to stabilization of the positive oxidized state of the T1 copper, in contrast stabilization of the neutral reduced state leads to a lower redox potential. Interestingly, ascorbate oxidase also has a negatively charged residue close to the T1 site and a relatively low redox potential (see above) [41].

McoP uses nitrous oxide as well as dioxygen as electron acceptor

Considering the recent hypothesis of Cozen *et al.* [14] that McoP could play a role in the denitrification pathway of *P. aerophilum*, we tested the catalytic reduction

Table 2. Copper content, molar coefficients and reduction potentials (E^0) of the T1 sites of McoP and mutants. The E^0-values were determined using the Nernst equation. ND, not determined.

Enzyme	Copper/protein ratio	$\varepsilon_{600\ nm}$ ($mM^{-1}·cm^{-1}$)	Redox potential (mV)
Wild type	3.2 ± 0.1	3.7	398
M297A	3.1 ± 0.3	3.6	400
M389A	3.4 ± 0.3	3.4	405
W355A	3.0 ± 0.1	3.8	ND
E296Q	3.1 ± 0.2	3.8	435

Table 3. Steady-state apparent kinetic constants for Cu^+ and ABTS for the different site-directed mutants. Reactions were performed at 40 °C in the presence of 0.1 mM $CuCl_2$.

	$K_{m\ app}$ (μM)		$k_{cat\ app}$ (min^{-1})		k_{cat}/K_m ($M^{-1}\cdot s^{-1}$)	
Enzyme	Cu^+	ABTS	Cu^+	ABTS	Cu^+	ABTS
Wild type	124 ± 22	133 ± 8	356 ± 32	72 ± 5	4.8×10^4	0.9×10^4
M297A	101 ± 5	106 ± 6	272 ± 4	23 ± 4	4.5×10^4	0.4×10^4
M389A	100 ± 27	100 ± 4	299 ± 13	20 ± 1	5.0×10^4	0.3×10^4
W355A	87 ± 7	100 ± 10	256 ± 9	52 ± 7	4.9×10^4	0.9×10^4
E296Q	110 ± 17	136 ± 18	300 ± 20	28 ± 2	4.5×10^4	0.4×10^4

of dioxygen, nitrous oxide and nitrite, using Fe^{2+} as electron donor. McoP is unable to reduce nitrite under the tested conditions, but it does reduce nitrous oxide and dioxygen at rates of 6.8 (± 0.5) and 3.8 (± 0.7) $\mu mol\cdot min^{-1}\cdot mg^{-1}$, respectively. Therefore, we conclude that McoP is kinetically competent to reduce nitrous oxide to molecular nitrogen and water, as well as dioxygen to water. In order to obtain further insight into the catalytic features of McoP, the reaction mechanisms for the reduction of nitrous oxide and dioxygen were investigated under steady-state conditions. Primary plots of $1/V_0$ versus 1/[S] for the oxidation of McoP by nitrous oxide or dioxygen (Fig. 8A,B) reveal parallel lines that are consistent with a ping-pong mechanism, which is in accordance with the previous findings reported for the laccases of the lacquer tree *Rhus vernicifera* and the fungus *Trametes villosa* [42,43]. The kinetic parameters of McoP for nitrous oxide and dioxygen were deduced by using the secondary plots of the line intercepts versus 1/[B] and slopes versus 1/[B], for which the following equations were used:

$$\frac{1}{V_o} = \frac{K_{mB}}{V_{max}}\frac{1}{[B]} + \frac{1}{V_{max}} \quad (1)$$

$$\frac{K_{mappA}}{V_o} = \frac{K_{mA}}{V_{max}} \quad (2)$$

V_o is the enzyme activity, and K_m is the affinity constant, either for A (reducing) or B (oxidizing) substrate. The obtained K_m values are similar for dioxygen (31 ± 0.2 μM) and nitrous oxide (33 ± 4 μM; Table 4). As expected, the K_m values for Fe^{2+} remain the same in reactions using either electron acceptor. However, the turnover rates are about three-fold higher for nitrous oxide as substrate than for dioxygen, and a higher efficiency was measured for nitrous oxide reduction than for dioxygen reduction. Therefore, McoP shows a preference for nitrous oxide as substrate. In analogous assays, we tested the N_2OR activity of the recombinant enzymes McoA from *A. aeolicus* and CotA laccase from *B. subtilis*. The metalloxidase McoA, under the tested conditions, is unable to use nitrous oxide as electron acceptor. Notably, CotA laccase is able to use nitrous oxide as electron acceptor, although with a 10-fold lower k_{cat} than that determined for dioxygen (in a reaction where ABTS was used instead of Fe^{2+} as the electron donor), clearly showing that dioxygen is its favorite substrate (Table 4).

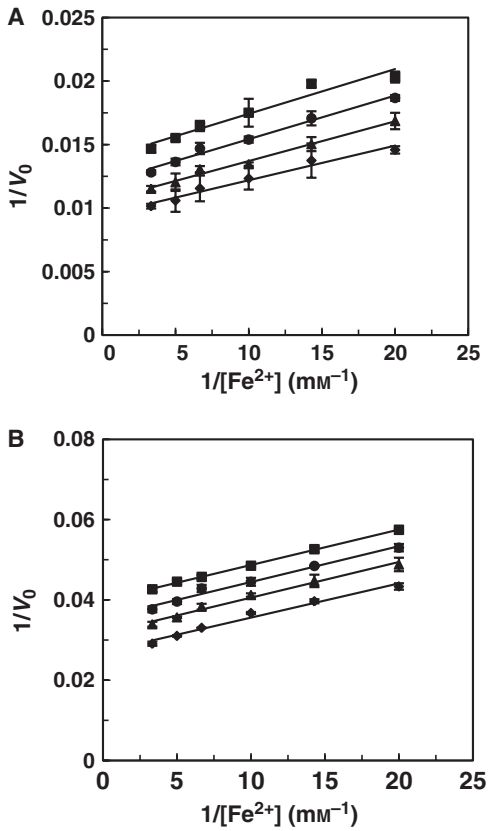

Fig. 8. Primary plots of $1/V_0$ against 1/[S] for McoP. Oxidation of Fe^{2+} at different concentrations of (A) N_2O and (B) O_2 (■, 50 μM; ●, 70 μM; ▲, 120 μM; ♦, 250 μM). V_0 and $[Fe^{2+}]$ are the initial rate of oxidation and concentration of reducing substrate, respectively. Error bars show sample standard deviation.

Table 4. Steady-state kinetic parameters for recombinant McoP from *P. aerophilum* and CotA laccase from *B. subtilis*, measured at 40 °C. Reactions were performed using either nitrous oxide or dioxygen as reducing substrate. Because of the different specificity for reducing substrates, Fe^{2+} was used in assays with McoP, and ABTS in reactions using CotA laccase.

Enzyme	Substrates		K_m (μM)	k_{cat} (s^{-1})	k_{cat}/K_m ($M^{-1}{\cdot}s^{-1}$)
McoP	Fe^{2+}/O_2	O_2	31 ± 0.2	3 ± 0.2	0.9×10^5
		Fe(II)	35 ± 0.2		0.9×10^5
	Fe^{2+}/N_2O	N_2O	32 ± 1.0	8 ± 2.0	3.0×10^5
		Fe(II)	33 ± 4.0		3.0×10^5
CotA	ABTS/O_2	O_2	37 ± 1.0	216 ± 6.0	58×10^5
		ABTS	109 ± 1.0		20×10^5
	ABTS/N_2O	N_2O	168 ± 0.3	21 ± 3.0	1.3×10^5
		ABTS	126 ± 2.0		1.7×10^5

Discussion

The hyperthermophilic archaeon *P. aerophilum* can use diverse respiratory pathways suggesting that this organism is able to respond to geochemical fluctuations within its native environments.

Unlike most hyperthermophilic archaeons, *P. aerophilum* can withstand the presence of oxygen, growing efficiently under microaerobic conditions. This fact explains the presence of a ORF in its genome, putatively assigned to an MCO, which is not found among its anaerobic close relatives. The dissimilatory reduction of nitrate to dinitrogen by *P. aerophilum* is relatively well studied; enzymatic activities of the denitrification pathway were detected in cellular fractions, and nitrate and nitric oxide reductases purified and characterized [13,17–19,22]. It is noteworthy that no recognizable homolog of *nosZ*, which codes for N_2OR in bacteria, has been found in the genome of this archaeon, indicating the existence of an alternative type of microbial N_2OR [23]. Interestingly, as in the case of *P. aerophilum*, the genomes of the denitrifying microorganisms *Nitrosomonas europea*, *Nitrosomonas euthropha*, *Haloferax volcanii* and *Haloarcula marismortui* lack the typical bacterial genes for nitrous oxide reduction [23]. Recently, DNA microarrays were used to compare genome expression patterns of *P. aerophilum* cultures supplemented with oxygen, nitrate, arsenate or ferric iron citrate as terminal electron acceptors [14]. These studies revealed an upregulation of gene *PAE1888*, coding for McoP, during nitrate respiration, suggesting a role for this MCO as an N_2OR. The present study provides experimental evidence that McoP is kinetically competent to use nitrous oxide as electron acceptor, providing further support for a role in the denitrification pathway of *P. aerophilum*. The specific activity of the recombinant McoP measured *in vitro* (6.8 $U{\cdot}mg^{-1}$ at 40 °C, which corresponds to 26 $U{\cdot}mg^{-1}$ at 85 °C, the optimal reaction temperature) lies in the middle of the range of values found for other N_2ORs from *Achromobacter cycloclastes*, *Pseudomonas nautica*, *Geobacillus thermodenitrificans*, or *Paracoccus denitrificans*, that show activities from 1.2 to 157 $U{\cdot}mg^{-1}$ [44–47]. Nevertheless, higher *in vivo* catalytic efficiency can be expected, as a result of the interaction with the putative physiological redox partner(s). McoP is most probably localized in the 'periplasmic' space between the cytoplasmic membrane and the surface layer of *P. aerophilum*, as its sequence contains a putative TAT-dependent signal peptide. The activities of the remaining denitrification pathway enzymes are localized in the membrane of *P. aerophilum* [17,18], therefore various small, mobile electron carriers (e.g. cytochromes or cupredoxins) that could possibly act as physiological electron donors for McoP are expected to be present in the membrane vicinity [44]. *P. aerophilum* does not have polyhemic *c*-type cytochromes, but its genome sequence contains two ORFs that code for putative *c*-type monohemic, cytochrome-containing proteins [15]. Nevertheless, as the substrate specificity of MCOs is quite broad, the nature of the physiological reductant of McoP is not clear at this point. For example, over 50 substrates have been identified in the reaction catalyzed by human ceruloplasmin, a mammalian MCO that is abundant in the serum and in interstitial fluid [48–50].

In spite of MCOs being promiscuous regarding the reducing substrates, dioxygen has been described as their the sole oxidant [1,2,9,40,51]. The main electron transfer steps in the reaction mechanism of MCOs are: (a) the reduction of the T1 site by the substrates; (b) the electron shuttle, through the Cys–His electron transfer pathway, to the trinuclear site; and (c) dioxygen reduction by the trinuclear site [9,10,51]. The trinuclear site is primed to bind dioxygen and generate bridged intermediates, but it also binds other exogenous ligands, such as nitric oxide, cyanide, fluoride, and azide [2,9,52]. The finding that McoP and CotA laccase from *B. subtilis* are able to couple the $4e^-/4H^+$ reduction of dioxygen to water, as well as the $2e^-/2H^+$ reduction of nitrous oxide to nitrogen and water, is quite interesting from the point of view of MCO enzymology, and raises new questions regarding the reaction mechanisms taking place at the trinuclear site of these enzymes. Coincidently, the microbial N_2ORs, whose kinetic and structural characteristics have been studied in most detail in bacteria of the genera *Pseudomonas*, *Paracoccus*, and *Achromobacter*, are homodimeric multicopper proteins [23,53]. The

crystal structures of N_2OR revealed that the copper ions are organized in two centers, a dicopper electron transfer and storage cluster, Cu_A, and the tetracopper sulfide center, Cu_Z; the former resembles the Cu_A found in cytochrome oxidases, and the latter is a novel mixed-valent copper center (Cu_4S) with a sulfide ion bridging a distorted tetrahedron of copper atoms [54–56]. This cluster is coordinated by seven His residues, and a water-derived ligand is proposed to bridge two of the copper atoms (Cu_I and Cu_{IV}), where substrate binds to the enzyme. It was proposed on the basis of the crystal structures that electrons enter at the mixed-valent binuclear Cu_A center of one subunit and are transferred over a 10 Å superexchange pathway to the Cu_Z cluster of a second subunit, where nitrous oxide reduction occurs [23,54,56]. Interestingly, copper nitrite reductases contain both T1 and T2 sites in their catalytic centers [20].

The efficiency of cuprous and ferrous ion oxidation by McoP is up to 10-fold higher than those observed for other metallo-oxidases, such as *E. coli* CueO, human ceruloplasmin, or yeast Fet3p [40,57]. These are reported to play a critical role in the maintenance of metal ion homeostasis in the respective organisms [1,40,57]. Analysis of the *P. aerophilum* genome shows that *mcoP* is not part of a putative metal-resistant determinant, as is the case of *cueO* in *E. coli* or *mcoA* in *A. aeolicus* [5,57]; however, McoP could probably act *in vivo* as a cytoprotector, because it has the catalytic competence to shift Cu^+ or Fe^{2+} towards the less toxic oxidized forms. Moreover, the enzymes from the MCO family are known as 'moonlighting' proteins, because they are able to change their functions in response to changes in concentration of their ligand/substrate, differential localization, and/or differential expression [58]. As an example, plausible physiological function(s) of human ceruloplasmin include copper transport, iron homeostasis, biogenic amine metabolism, and defense against oxidative stress [58].

In conclusion, this work provided the spectroscopic, biochemical and kinetic characterization of a unique hyperthermostable MCO that exhibits a higher specificity for nitrous oxide than for dioxygen, representing a novel N_2OR. *P. aerophilum* thrives in geothermally and volcanically heated habitats, in which potentially cytotoxic metals are usually abundant. In accordance with this, McoP is a thermoactive and thermostable metallo-oxidase showing high efficiency in the oxidation of toxic transition metals. Work is in progress to determine the crystallographic structure of this enzyme, which will help in the dissection of its unusual properties.

Experimental procedures

Cloning *mcoP* in *Escherichia coli*

The *mcoP* gene was amplified by PCR, using oligonucleotides *mcoP*-191D (5′-CTCAGCCATATGATCACTAGAAGG-3′) and *mcoP*-15R (5′-CTCTTCCTCGAGCGGATTATTTAA C-3′). The 1543 bp PCR product was digested with *Nde*I and *Xho*I, and inserted between the same restriction sites of plasmid pET-15b (Novagen) to yield pATF-20, allowing the expression of *mcoP* with a His_6-tag fusion to the N-terminus. The expression strain *E. coli* Tuner (DE3) (Novagen, Darmstadt, Germany) was freshly transformed with pG-KJE8 (Cm^r) (from Takara Bio Inc., Kyoto, Japan) before being transformed with the recombinant plasmid pATF-20. In pG-KJE8, the L-arabinose-inducible promoter (*araB*) was used to express the *dnak/dnaJ/grpE* chaperones, and the *Pzt-1* (tet) promoter to regulate the expression of *groES/groEL* chaperones. The coexpression of chaperones with *mcoP* enables the overproduction of soluble McoP.

Site-directed mutagenesis

Single amino acid substitutions in McoP were created using the QuikChange site-directed mutagenesis kit (Stratagene, Santa Clara, CA, USA). Plasmid pATF-20 (containing the wild-type *mcoP* sequence) was used as template, and primers *mcoP*M297Ad (5′-CCCATGCATTTAGAAGCGGGC CACGG-3′) and *mcoP*M297Ar (5′-CCGTGGCCCGCTT CTAAATGCATGGG-3′) were used to generate the M297A mutation, primers *mcoP*M389Ad (5′-CAAGGCGTCTGC GCCCCACCCTATC-3′) and *mcoP*M389Ar (5′-GATAG GGTGGGGCGCAGACGCCTTG-3′) were used to generate the M389A mutation, primers *mcoP*E296Qd (5′-CCCATGCATTTACAAATGGGCCACGGG-3′) and *mcoP*E296Qr (5′-CCCGTGGCCCATTTGTAAATGCATG GG-3′) were used to generate the E296Q mutation, and primers mcoPW355Ad (5′-GGAATGCAGGCGACGA TAAACGGC-3′) and mcoPW355Ar (5′-GCCGTTTATC GTCGCCTGCATTCC-3′) were used to generate the W355A mutation. The presence of the desired mutations in the resulting plasmids, pATF-27 (carrying the M297A mutation), pATF-28 (bearing the E296Q mutation), pATF-33 (carrying the M389A mutation), and pATF-34 (carrying the W355A mutation), and the absence of unwanted mutations in other regions of the insert were confirmed by DNA sequence analysis. These plasmids were introduced into the *E. coli* Tuner expression strain, along with plasmid pG-KJE8, as mentioned above.

Overproduction and purification of recombinant proteins

The expression strains were grown in LB culture medium supplemented with ampicillin (100 $\mu g \cdot mL^{-1}$),

cloramphenicol (34 μg·mL^{-1}), arabinose (1 mg·mL^{-1}) and tetracycline (1 ng·mL^{-1}) at 30 °C. Growth was followed up to $D_{600\ nm}$ = 0.6, at that point 100 μM isopropyl thio-β-D-galactoside and 250 μM $CuCl_2$ were added to the culture medium, and the temperature was lowered to 25 °C. Incubation was continued for a further 4 h, when a change in the microaerobic conditions was achieved [35]. Cells were harvested by centrifugation (8000 ***g***, 10 min, 4 °C) after a further 20 h of growth. The cell sediment was suspended in 20 mM phosphate buffer (pH 7.4) with 100 mM NaCl, containing DNase I (10 μg·mL^{-1} extract), $MgCl_2$ (5 mM), and a mixture of protease inhibitors, antipain and leupeptin (2 μg·mL^{-1} extract). Cells were disrupted in a French press cell (at 19 000 p.s.i.) and centrifuged (18 000 ***g***, 60 min, 4 °C) to remove cell debris. The cell lysate was then loaded onto a 1 mL HisTrap HP column (GE Healthcare, Waukesha, WI, USA) equilibrated with 20 mM phosphate buffer (pH 7.4) supplemented with 100 mM NaCl. Elution was carried out with a one-step linear imidazole (500 mM) gradient of 40 mL in the same buffer. The active fractions were pooled out and concentrated before being applied to a Superdex 75 HR 10/30 column (GE Healthcare) equilibrated with 20 mM Tris/HCl buffer (pH 7.6) with 0.2 M NaCl. All purification steps were carried out at room temperature in an AKTA purifier (GE Healthcare). The His-tag was subsequently removed by using the Thrombin Digestion kit (Novagen, Darmstadt, Germany).

Spectroscopic analysis

Spectroscopic analyses of the protein samples were routinely performed after incubation with the oxidizing agent potassium iridate followed by dialysis. The UV–visible spectra were recorded at room temperature in 20 mM Tris/HCl buffer (pH 7.6), in the presence of 200 mM NaCl. CD in the far UV was measured on a Jasco-815 spectropolarimeter, using a protein content of 25 μM in highly pure water (Mili-Q), as described previously [5]. RR spectra were measured as previously described, with 568 nm excitation [12]. The fitted band intensities and frequencies were used for determination of the intensity-weighted frequency $< \nu_{Cu-S} >$ continuous wave X band. EPR measurements were carried out with a Bruker E500 Elexsys Series, using the Bruker ER 4122 SHQE cavity and an Oxford helium continuous flow cryostat (ESR900). EPR samples were prepared by adding increasing quantities of exogenous copper ($CuCl_2$) to the enzyme solution, to give a final concentration of 196 μM. Recombinant McoP was also incubated with exogenous copper to yield a final protein/copper ratio of 1 : 5, and a final protein concentration of 122 μM. The EPR spectra of McoP were recorded at 70 K with 0.5 mT modulation amplitude, 100 kHz modulation frequency, and 2 mW microwave power (ν = 9.396 GHz). The EPR spectra were baseline-corrected and simulated using software for fitting EPR frozen solution spectra that is a modified version of a program written by J. R. Pilbrow (CUSIMNE) [59].

Redox titrations

Redox titrations performed at 25 °C and pH 7.6, under an argon atmosphere, were monitored by visible spectroscopy (300–900 nm) in a Shimadzu Multispec-1501 spectrophotometer. The reaction mixture contained 25–50 μM enzyme in 20 mM Tris/HCl buffer (pH 7.6) and the following mediators at 10 μM final concentration each (reduction potential in parentheses): 1,2-naphthoquinone-4-sulfonic acid (+215 mV), dimethyl-*p*-phenylenediamine (+344 mV), monocarboxylic acid ferrocene (+530 mV), 1,1′-dicarboxylic acid ferrocene (+644 mV), and Fe^{2+}/Fe^{3+}-Tris-(1,10-phenanthroline) (+1070 mV). Potassium hexachloroiridate(IV) was used as oxidant, and sodium dithionite as reductant. The redox potential measurements were performed with a silver/silver chloride electrode, calibrated with a quinhydrone-saturated solution at pH 7.0. The redox potentials are quoted with respect to the standard hydrogen electrode.

Substrate specificities and kinetics

The catalytic properties of McoP were measured in the presence of oxygen, using four different reducing substrates: two aromatic, the nonphenolic ABTS and the phenolic SGZ, and two metals, Cu^+ and Fe^{2+}. This was performed at 40 °C, as technical limitations prevented Cu^+ oxidation measurements at higher temperatures. The effect of pH on the enzyme activity was determined for ABTS and SGZ in Britton–Robinson buffer (a 100 mM boric acid/100 mM phosphoric acid/100 mM acetic acid mixture titrated to the desired pH with 0.5 M NaOH), as previously described [11]. For measurements with metal ions, the pH was chosen in accordance with the stability of the metal ions in solution; pH 3.5 for Cu^+ and pH 5 for Fe^{2+}. The oxidation of ABTS, SGZ and ferrous ammonium sulfate was spectrophotometrically monitored with either a Nicolet Evolution 300 spectrophotometer (Thermo Industries, Waltham, MA, USA) or a Sinergy 2 microplate reader with a 96-well plate (BioTek, Winooski, VT, USA). Cu^+ oxidation activity was measured in terms of oxygen consumption rates by using an oxygraph, as previously described [5]. The optimal temperature for the activity was determined for ABTS at temperatures ranging from 30 to 90 °C. Apparent kinetic parameters were determined using reaction mixtures containing Cu^+ (10–300 μM, pH 3.5), Fe^{2+} (5–70 μM, pH 5), ABTS (10–200 μM, pH 3) and SGZ (1–100 μM, pH 7). The apparent kinetic constants K_m and k_{cat} were fitted directly to the Michaelis–Menten equation (ORIGINLAB software, Northampton, MA, USA). All enzymatic assays were performed at least in triplicate. The second-order kinetic

analysis with Fe^{2+} (as reducing substrate) and nitrous oxide and dioxygen (as oxidizing substrates) was spectrophotometrically assayed by monitoring the oxidation of Fe^{2+} at 315 nm. The cuvettes (1 mL) containing 100 mM Britton–Robinson buffer at pH 5 and 300 μM Fe^{2+} were sealed with rubber stoppers and made anaerobic with argon bubbling. A saturated solution of dioxygen (1 mM) and nitrous oxide (25 mM) was prepared by bubbling Milli-Q water in a sealed serum bottle with oxygen or nitrous oxide gas [46]. The kinetic constants for nitrous oxide, dioxygen and Fe^{2+} were determined by varying the concentrations of the reducing and oxidizing substrate, as described elsewhere [42].

Thermal stability

Kinetic stability was determined as previously described by Martins *et al.* [6]. Briefly, the enzyme was incubated at 80 °C, and tested for activity at 40 °C, with ABTS as the substrate, at fixed time intervals. DSC was carried out in a VP-DSC instrument from MicroCal at a scan rate of 60 °C·h^{-1}. The experimental calorimetric trace was obtained at pH 3 (50 mM glycine buffer) after baseline correction (buffer alone). The resulting DSC trace was analyzed with the DSC software built within the ORIGINLAB spreadsheet to obtain the transition excess heat capacity function (a cubic polynomial function was used to fit the shift in baseline associated with unfolding).

Comparative modeling

The structural model of *P. aerophilum* McoP was derived by using comparative modeling methods, with the program MODELLER [60], release 9v3. For this, both *E. coli* CueO [31] (Protein Data Bank code: 1KV7) and *B. subtilis* CotA [3] (Protein Data Bank code: 1GSK) structures, which show 29.0% and 23.1% sequence identity, respectively, were chosen as templates. These templates were first structurally aligned, providing a profile against which the McoP sequence was aligned with the ALIGN2D feature of MODELLER. This sequence alignment, together with the two known structures, was the basis for deriving an initial structural model of McoP. Then, the alignment was changed in an iterative process, and new structural models were derived until its quality, assessed using the program PROCHECK [61], was found to be satisfactory. After loop refinement, the final model presented 89.1% of the residues in the most favored regions of the Ramachandran plot, 10.9% in the additional allowed regions, and no residues in the generously allowed or disallowed regions.

Other methods

The copper content was determined through the trichloroacetic acid/bicinchoninic acid method [62]. The protein concentration was measured by using the absorbance band at 280 nm (ε_{280} = 57 750 M^{-1}·cm^{-1}) or the Bradford assay [63], using BSA as standard.

Acknowledgements

E. P. Melo is gratefully acknowledged for helpful discussions. This work was supported by a project grant from the European Commission (BIORENEW-FP6-2004-NMP-NI-4/026456). A. T. Fernandes and J. M. Damas hold PhD fellowships from the Fundação para a Ciência e Tecnologia, Portugal (SFRH/BD/31444/2006 and SFRH/BD/41316/2007, respectively).

References

1 Lindley PF (2001) Multi-copper oxidases. In *Handbook on Metalloproteins* (Bertini I, Sigel A & Sigel H eds), pp 763–811. Marcel Dekker, New York.
2 Solomon EI, Sundaram UM & Machonkin TE (1996) Multicopper oxidases and oxygenases. *Chem Rev* **96**, 2563–2606.
3 Enguita FJ, Martins LO, Henriques AO & Carrondo MA (2003) Crystal structure of a bacterial endospore coat component. A laccase with enhanced thermostability properties. *J Biol Chem* **278**, 19416–19425.
4 Fernandes AT, Martins LO & Melo EP (2009) The hyperthermophilic nature of the metallo-oxidase from *Aquifex aeolicus*. *Biochim Biophys Acta* **1794**, 75–83.
5 Fernandes AT, Soares CM, Pereira MM, Huber R, Grass G & Martins LO (2007) A robust metallo-oxidase from the hyperthermophilic bacterium *Aquifex aeolicus*. *FEBS J* **274**, 2683–2694.
6 Martins LO, Soares CM, Pereira MM, Teixeira M, Costa T, Jones GH & Henriques AO (2002) Molecular and biochemical characterization of a highly stable bacterial laccase that occurs as a structural component of the *Bacillus subtilis* endospore coat. *J Biol Chem* **277**, 18849–18859.
7 Pereira L, Coelho AV, Viegas CA, Ganachaud C, Iacazio G, Tron T, Robalo MP & Martins LO (2009) On the mechanism of biotransformation of the anthraquinonic dye blue 62 by laccases. *Adv Synth Catal* **351**, 1857–1865.
8 Pereira L, Coelho AV, Viegas CA, Santos MM, Robalo MP & Martins LO (2009) Enzymatic biotransformation of the azo dye Sudan Orange G with bacterial CotA-laccase. *J Biotechnol* **139**, 68–77.
9 Bento I, Martins LO, Lopes GG, Carrondo MA & Lindley PF (2005) Dioxygen reduction by multi-copper oxidases; a structural perspective. *Dalton Trans* **7**, 3507–3513.

10 Chen Z, Durao P, Silva CS, Pereira MM, Todorovic S, Hildebrandt P, Bento I, Lindley PF & Martins LO (2010) The role of Glu498 in the dioxygen reactivity of CotA-laccase from *Bacillus subtilis*. *Dalton Trans* **39**, 2875–2882.
11 Durao P, Bento I, Fernandes AT, Melo EP, Lindley PF & Martins LO (2006) Perturbations of the T1 copper site in the CotA laccase from *Bacillus subtilis*: structural, biochemical, enzymatic and stability studies. *J Biol Inorg Chem* **11**, 514–526.
12 Durao P, Chen Z, Silva CS, Soares CM, Pereira MM, Todorovic S, Hildebrandt P, Bento I, Lindley PF & Martins LO (2008) Proximal mutations at the type 1 copper site of CotA laccase: spectroscopic, redox, kinetic and structural characterization of I494A and L386A mutants. *Biochem J* **412**, 339–346.
13 Fitz-Gibbon ST, Ladner H, Kim UJ, Stetter KO, Simon MI & Miller JH (2002) Genome sequence of the hyperthermophilic crenarchaeon *Pyrobaculum aerophilum*. *Proc Natl Acad Sci USA* **99**, 984–989.
14 Cozen AE, Weirauch MT, Pollard KS, Bernick DL, Stuart JM & Lowe TM (2009) Transcriptional map of respiratory versatility in the hyperthermophilic crenarchaeon *Pyrobaculum aerophilum*. *J Bacteriol* **191**, 782–794.
15 Feinberg LF & Holden JF (2006) Characterization of dissimilatory Fe(III) versus NO_3^- reduction in the hyperthermophilic archaeon *Pyrobaculum aerophilum*. *J Bacteriol* **188**, 525–531.
16 Feinberg LF, Srikanth R, Vachet RW & Holden JF (2008) Constraints on anaerobic respiration in the hyperthermophilic Archaea *Pyrobaculum islandicum* and *Pyrobaculum aerophilum*. *Appl Environ Microbiol* **74**, 396–402.
17 Afshar S, Kim C, Monbouquette HG & Schroder II (1998) Effect of tungstate on nitrate reduction by the hyperthermophilic archaeon *Pyrobaculum aerophilum*. *Appl Environ Microbiol* **64**, 3004–3008.
18 de Vries S, Strampraad MJ, Lu S, Moenne-Loccoz P & Schroder I (2003) Purification and characterization of the MQH2:NO oxidoreductase from the hyperthermophilic archaeon *Pyrobaculum aerophilum*. *J Biol Chem* **278**, 35861–35868.
19 Volkl P, Huber R, Drobner E, Rachel R, Burggraf S, Trincone A & Stetter KO (1993) *Pyrobaculum aerophilum* sp. nov., a novel nitrate-reducing hyperthermophilic archaeum. *Appl Environ Microbiol* **59**, 2918–2926.
20 Tavares P, Pereira AS, Moura JJ & Moura I (2006) Metalloenzymes of the denitrification pathway. *J Inorg Biochem* **100**, 2087–2100.
21 Zumft WG (1997) Cell biology and molecular basis of denitrification. *Microbiol Mol Biol Rev* **61**, 533–616.
22 Afshar S, Johnson E, de Vries S & Schroder I (2001) Properties of a thermostable nitrate reductase from the hyperthermophilic archaeon *Pyrobaculum aerophilum*. *J Bacteriol* **183**, 5491–5495.
23 Zumft WG & Kroneck PM (2007) Respiratory transformation of nitrous oxide (N_2O) to dinitrogen by Bacteria and Archaea. *Adv Microb Physiol* **52**, 107–227.
24 Uthandi S, Saad B, Humbard MA & Maupin-Furlow JA (2010) LccA, an archaeal laccase secreted as a highly stable glycoprotein into the extracellular medium by *Haloferax volcanii*. *Appl Environ Microbiol* **76**, 733–743.
25 Sreerama N, Venyaminov SY & Woody RW (1999) Estimation of the number of alpha-helical and beta-strand segments in proteins using circular dichroism spectroscopy. *Protein Sci* **8**, 370–380.
26 Blair DF, Campbell GW, Cho WK, English AM, Fry HA, Lum V, Norton KA, Schoonover JR & Chan SI (1985) Resonance Raman studies of blue copper proteins: effects of temperature and isotopic substitutions. Structural and thermodynamic implications. *J Am Chem Soc* **107**, 5755–5766.
27 Green MT (2006) Application of Badger's rule to heme and non-heme iron–oxygen bonds: an examination of ferryl protonation states. *J Am Chem Soc* **128**, 1902–1906.
28 Pogni R, Brogioni B, Baratto MC, Sinicropi A, Giardina P, Pezzella C, Sannia G & Basosi R (2007) Evidence for a radical mechanism in biocatalytic degradation of synthetic dyes by fungal laccases mediated by violuric acid. *Biocatal Biotransformation* **25**, 269–275.
29 Solomon EI, Baldwin MJ & Lowery MD (1992) Electronic structures of active sites in copper proteins: contributions to reactivity. *Chem Rev* **92**, 521–542.
30 DeLano WL (2003) *The PyMOL Molecular Graphics System*. DeLano Scientific, Palo Alto, CA.
31 Roberts SA, Weichsel A, Grass G, Thakali K, Hazzard JT, Tollin G, Rensing C & Montfort WR (2002) Crystal structure and electron transfer kinetics of CueO, a multicopper oxidase required for copper homeostasis in *Escherichia coli*. *Proc Natl Acad Sci USA* **99**, 2766–2771.
32 Miyazaki K (2005) A hyperthermophilic laccase from *Thermus thermophilus* HB27. *Extremophiles* **9**, 415–425.
33 Savini I, D'Alessio S, Giartosio A, Morpurgo L & Avigliano L (1990) The role of copper in the stability of ascorbate oxidase towards denaturing agents. *Eur J Biochem* **190**, 491–495.
34 Bonaccorsi di Patti MC, Musci G, Giartosio A, D'Alessio S & Calabrese L (1990) The multidomain structure of ceruloplasmin from calorimetric and limited proteolysis studies. *J Biol Chem* **265**, 21016–21022.
35 Durao P, Chen Z, Fernandes AT, Hildebrandt P, Murgida DH, Todorovic S, Pereira MM, Melo EP & Martins LO (2008) Copper incorporation into recombinant CotA laccase from *Bacillus subtilis*: characteriza-

tion of fully copper loaded enzymes. *J Biol Inorg Chem* **13**, 183–193.
36 Xu F (1997) Effects of redox potential and hydroxide inhibition on the pH activity profile of fungal laccases. *J Biol Chem* **272**, 924–928.
37 Singh SK, Grass G, Rensing C & Montfort WR (2004) Cuprous oxidase activity of CueO from *Escherichia coli*. *J Bacteriol* **186**, 7815–7817.
38 Stoj C & Kosman DJ (2003) Cuprous oxidase activity of yeast Fet3p and human ceruloplasmin: implication for function. *FEBS Lett* **554**, 422–426.
39 Hall SJ, Hitchcock A, Butler CS & Kelly DJ (2008) A multicopper oxidase (Cj1516) and a CopA homologue (Cj1161) are major components of the copper homeostasis system of *Campylobacter jejuni*. *J Bacteriol* **190**, 8075–8085.
40 Kosman DJ (2010) Multicopper oxidases: a workshop on copper coordination chemistry, electron transfer, and metallophysiology. *J Biol Inorg Chem* **15**, 15–28.
41 Quintanar L, Stoj C, Taylor AB, Hart PJ, Kosman DJ & Solomon EI (2007) Shall we dance? How a multicopper oxidase chooses its electron transfer partner. *Acc Chem Res* **40**, 445–452.
42 Bukh C, Lund M & Bjerrum MJ (2006) Kinetic studies on the reaction between *Trametes villosa* laccase and dioxygen. *J Inorg Biochem* **100**, 1547–1557.
43 Petersen LC & Degn H (1978) Steady-state kinetics of laccase from *Rhus vernicifera*. *Biochim Biophys Acta* **526**, 85–92.
44 Dell'acqua S, Pauleta SR, Monzani E, Pereira AS, Casella L, Moura JJ & Moura I (2008) Electron transfer complex between nitrous oxide reductase and cytochrome c552 from *Pseudomonas nautica*: kinetic, nuclear magnetic resonance, and docking studies. *Biochemistry* **47**, 10852–10862.
45 Fujita K, Chan JM, Bollinger JA, Alvarez ML & Dooley DM (2007) Anaerobic purification, characterization and preliminary mechanistic study of recombinant nitrous oxide reductase from *Achromobacter cycloclastes*. *J Inorg Biochem* **101**, 1836–1844.
46 Kristjansson JK & Hollocher TC (1980) First practical assay for soluble nitrous oxide reductase of denitrifying bacteria and a partial kinetic characterization. *J Biol Chem* **255**, 704–707.
47 Liu X, Gao C, Zhang A, Jin P, Wang L & Feng L (2008) The *nos* gene cluster from gram-positive bacterium *Geobacillus thermodenitrificans* NG80-2 and functional characterization of the recombinant NosZ. *FEMS Microbiol Lett* **289**, 46–52.
48 Frieden E & Hsieh HS (1976) The biological role of ceruloplasmin and its oxidase activity. *Adv Exp Med Biol* **74**, 505–529.
49 Hellman NE & Gitlin JD (2002) Ceruloplasmin metabolism and function. *Annu Rev Nutr* **22**, 439–458.
50 Young SN & Curzon G (1972) A method for obtaining linear reciprocal plots with caeruloplasmin and its application in a study of the kinetic parameters of caeruloplasmin substrates. *Biochem J* **129**, 273–283.
51 Solomon EI, Augustine AJ & Yoon J (2008) O_2 reduction to H_2O by the multicopper oxidases. *Dalton Trans* **14**, 3921–3932.
52 Wilson MT & Torres J (2004) Reactions of nitric oxide with copper containing oxidases; cytochrome c oxidase and laccase. *IUBMB Life* **56**, 7–11.
53 Solomon EI, Sarangi R, Woertink JS, Augustine AJ, Yoon J & Ghosh S (2007) O_2 and N_2O activation by bi-, tri-, and tetranuclear Cu clusters in biology. *Acc Chem Res* **40**, 581–591.
54 Brown K, Djinovic-Carugo K, Haltia T, Cabrito I, Saraste M, Moura JJ, Moura I, Tegoni M & Cambillau C (2000) Revisiting the catalytic CuZ cluster of nitrous oxide (N_2O) reductase. Evidence of a bridging inorganic sulfur. *J Biol Chem* **275**, 41133–41136.
55 Haltia T, Brown K, Tegoni M, Cambillau C, Saraste M, Mattila K & Djinovic-Carugo K (2003) Crystal structure of nitrous oxide reductase from *Paracoccus denitrificans* at 1.6 A resolution. *Biochem J* **369**, 77–88.
56 Paraskevopoulos K, Antonyuk SV, Sawers RG, Eady RR & Hasnain SS (2006) Insight into catalysis of nitrous oxide reductase from high-resolution structures of resting and inhibitor-bound enzyme from *Achromobacter cycloclastes*. *J Mol Biol* **362**, 55–65.
57 Stoj CS & Kosman DJ (2005) Copper proteins: oxidases. In *Encyclopedia of Inorganic Chemistry* (King BR ed), pp 1134–1159. John Wiley & Sons, New York, NY.
58 Bielli P & Calabrese L (2002) Structure to function relationships in ceruloplasmin: a 'moonlighting' protein. *Cell Mol Life Sci* **59**, 1413–1427.
59 Rakhit G, Antholine WE, Froncisz W, Hyde JS, Pilbrow JR, Sinclair GR & Sarkar B (1985) Direct evidence of nitrogen coupling in the copper(II) complex of bovine serum albumin by S-band electron spin resonance technique. *J Inorg Biochem* **25**, 217–224.
60 Sali A (1995) Comparative protein modeling by satisfaction of spatial restraints. *Mol Med Today* **1**, 270–277.
61 Laskowski RA, MacArthur MW, Moss DS & Thornton JM (1993) Procheck – a Program to check the stereochemical quality of protein structures. *J Appl Crystallogr* **26**, 283–291.
62 Brenner AJ & Harris ED (1995) A quantitative test for copper using bicinchoninic acid. *Anal Biochem* **226**, 80–84.

63 Bradford MM (1976) A rapid and sensitive method for the quantification of microgram quantities of protein utilizing the principle of protein-dye binding. *Anal Biochem* **72**, 248–254.

Supporting information

The following supplementary material is available:
Table S1. Purification of recombinant McoP produced in *Escherichia coli*.
Fig. S1. SDS/PAGE analysis of McoP overproduction and purification.
Fig. S2. CD spectrum in the far-UV region, reflecting the typical secondary structure of multicopper oxidases, rich in β-sheets, with a negative peak at 213–214 nm.

This supplementary material can be found in the online version of this article.

Please note: As a service to our authors and readers, this journal provides supporting information supplied by the authors. Such materials are peer-reviewed and may be re-organized for online delivery, but are not copy-edited or typeset. Technical support issues arising from supporting information (other than missing files) should be addressed to the authors.